Tight-binding calculations of the elastic constants and phonons of hcp Zr: Complications due to anisotropic stress and long-range forces

I. Schnell,[1] M. D. Jones,[2] S. P. Rudin,[1] and R. C. Albers[1]

[1]*Theoretical Division, Los Alamos National Laboratory, Los Alamos, New Mexico 87545, USA*

[2]*Department of Physics and Center for Computational Research, University at Buffalo, The State University of New York, Buffalo, New York 14260, USA*

We have calculated the phonons and elastic constants of zirconium in the hexagonal-close-packed (hcp) crystal structure using the Naval Research Laboratory (NRL) empirical tight-binding (TB) approach; the tight-binding parameters are obtained by fitting to *ab initio* density-functional theory–generalized gradient approximation energy bands and total energies for many different structures and volumes. We address difficulties involved with the fitting procedure and give results for elastic constants, force constants, quasiharmonic phonons, and specific heat. Because the predicted TB lattice constants at the zero-temperature energy minimum are slightly different from those experimentally observed at room temperature, our TB model has an anisotropic stress at the experimental lattice constants. We correct for these stresses in our calculations of the elastic constants and sound speeds. Such techniques are also useful for calculating such properties for arbitrary c/a. Our phonon calculations were done by the direct-force method in real space using calculated force constants; these fall off quite slowly with distance, which causes problems with the calculated phonon spectrum due to the slow convergence with increasing supercell size. This long-range behavior could play a large role in determining the unusually anharmonic and anomalous physical properties of Zr. We show that similar, although less severe, problems should arise for other metals. These considerations suggest that the direct-force method for calculating phonons may be problematic for many metals.

I. INTRODUCTION

Density-functional theory (DFT) calculations based on the generalized gradient approximation (GGA) (Ref. 1) are an effective tool for studying the properties of many systems at zero temperature, ranging from bulk materials to clusters and surfaces. With the availability of increasingly powerful computers and efficient algorithms, it is now possible to perform calculations for reasonably large systems. Despite these advances, the application of *ab initio* methods to the study of finite-temperature thermodynamic effects such as thermal expansion and phase diagrams remains challenging, since such effects involve lattice contributions to the free energy that can be difficult to evaluate, especially if anharmonic contributions are important. The goal of this work is to explore the finite-temperature properties of a complicated electronic material, Zr, by using a tight-binding approach to calculate the phonon spectrum and related properties. Although first-principles methods based on band-structure approaches have been used to directly calculate the zero-temperature phonons for some materials, we have instead focused on a tight-binding approach in order to greatly speed up the calculations. We should like ultimately to be able to calculate phase diagrams, strong anharmonicities, and other complex materials properties that are still too computationally expensive with direct full-potential electronic structure methods.

We have previously had some success in using tight-binding methods on simpler materials (Cu metal[2] and Ti metal[3]). The tight-binding method works extremely well for Cu, with an accurate description of the phonon spectrum and good agreement with experiment for many different thermodynamic and physical properties. However, Cu has a nearly filled d-electron shell, and for many properties more closely resembles an s-p metal. Its phase diagram is very simple (with no solid-solid phase transformations below 188 GPa at room temperature). As a second test of the tight-binding methodology, we therefore tested Ti, which is just above Zr in the periodic table. Ti has a partially filled d shell and has a rich phase diagram. Although the predicted phonon spectrum for Ti was worse than for that of Cu, the hcp-to-ω phase transformation was well described by tight binding. As we discuss below, Zr is an extremely challenging material with many anomalies, which we believe is a far more rigorous test, perhaps an extreme example, to see how accurately a tight-binding approach can work. Although we have recently shown that the methods described in this paper provide a reasonably accurate prediction for some of the phase boundaries in Zr,[4] there are also some important difficulties that must be considered, which we explain in great detail in this paper.

At normal pressure and room temperature, Zr has a hexagonal-close-packed (hcp) crystal structure. For a complete description, it is therefore useful to be able to calculate both phonons and elastic constants for arbitrary c/a. This requires calculations for a crystal structure with anisotropic stress. In this paper we illustrate how to do this for Zr at the experimental lattice constants, which represent a stressed system in our tight-binding model. In addition, we show that the force constants of Zr fall off slowly with distance, causing supercell convergence problems when direct-force methods are used to calculate the phonon spectrum. It is likely that these problems are related to the many anomalous properties of Zr.

The thermodynamic properties of zirconium have been the subject of many experimental and theoretical studies.[5–9]

At room temperature and ambient pressure, the stable crystalline state of this early 4d transition metal is a hexagonal-close-packed (hcp) structure (the α phase). When the temperature is raised, at zero pressure, Zr transforms martensitically into the bcc structure (the β phase) at 1136 K, and then eventually melts out of the bcc phase. When the pressure is increased at room temperature, a martensitic phase transformation into the ω phase is observed between 3.3 and 6.7 GPa.[10] At even higher pressure, 30 GPa, Zr exhibits a martensitic transformation into the bcc structure.[5]

More important for this work, however, are the anomalous phonon properties of Zr, which might be precursors to the various martensitic phase transformations.[11] At high temperatures, the bcc phonons show a large strongly temperature-dependent low-energy dip in the high-symmetry longitudinal phonon branch $L [\xi,\xi,\xi]$ for $\xi=2/3$, which is related to the ω phase transformation. The entire transverse (T_1) phonon branch from Γ out to the N point of the Brillouin zone is also anomalously low, which is related to the transformation into the hcp structure. In the hcp crystal structure, the zone center of the [001] LO branch softens appreciably, and exhibits a dip at low temperatures,[7] which may be related to the superconducting transition. The hcp elastic constants also have a marked anisotropy in the temperature dependence of the shear moduli.[6] These phonon properties are a sign of strong anharmonicity and indicate the need for better models for the atomic forces in Zr.

As a first step towards calculating these anharmonicities, we have used the NRL tight-binding (TB) approach[12] to calculate the zero-temperature phonons within the quasiharmonic approximation for the hcp structure, as well as the specific heat at constant volume. Our approach is first-principles in the sense that the tight-binding parameters are based on *ab initio* band-structure calculations and do not depend upon experimental data. Finite-temperature results are determined by thermally populating the quasiharmonic phonons, and calculating the free energy from these. Since the quasiharmonic phonons are calculated at zero temperature, in this paper we cannot, unfortunately, address the temperature dependence of the phonons themselves, and only limited temperature-dependent anharmonic effects. However, the long-term hope is that tight-binding methods will be sufficiently fast, flexible, and accurate to ultimately enable such studies.

This paper is organized as follows. In Sec. II, we explain the tight-binding approach that we use in this paper, and discuss how to determine the necessary parameters. In Sec. III, we present calculations of the Zr phonons from the tight-binding calculations and compare with experiment. Because sound velocities are equivalent to the large wavelength (small q) limit of the phonon spectrum, and depend only on the elastic constants, in Sec. IV we provide calculations for the elastic constants and in Sec. V for the sound velocities. We also explain the effects of stress on these properties, since the lattice constants and c/a for the tight-binding predictions for equilibrated Zr are slightly different from the experimental values, and hence calculations at the experimental lattice constants require theoretical calculations for Zr under the small applied stress that is needed to shift the Zr

lattice constants away from their theoretical minimum. In Sec. VI we discuss a more explicit relationship (Born-Huang) between the dynamical phonon matrix and the elastic constants, and in Sec. VII the anomalously slow decay of the force constants with distance, which we believe is responsible for many of the unusual properties of Zr. A comparison with the experimental specific heat is given in Sec. VIII. Finally, our results are summarized in Sec. IX.

II. TIGHT-BINDING APPROACH AND FITTING PROCEDURE

In this work, we use the Naval Research Laboratory (NRL) tight-binding approach.[12] This method is designed to reproduce *ab initio* DFT calculations by fitting the model parameters to DFT band structures and total energies. Being a parametrized version of the DFT calculations, the method is computationally orders of magnitude faster than DFT itself. The ultimate goal is to find a tight-binding parametrization that has the accuracy and transferability of the *ab initio* calculations without the huge computational expense.

The total DFT energy is given by ($i=\{\mathbf{k},n\}$)

$$E[n] = \sum_i f(\epsilon_i - \mu)\epsilon_i + F[n], \qquad (1)$$

i.e., a sum over the energy eigenvalues ϵ_i that are weighted with the Fermi function $f(z)=1/(1+e^{\beta z})$ plus a remaining density functional $F[n]$, which contains (i) the ion-ion interaction energy, (ii) parts of the Hartree and exchange energy not yet included in the sum, and (iii) corrections for double counting. In the NRL-TB model, the Kohn-Sham potential (as well as the eigenvalues ϵ_i) are shifted by $V_0=F[n]/N_e$, such that $E[n]=\Sigma_i f(\epsilon_i'-\mu')\epsilon_i'$. The shifted ϵ_i' are considered functions of only the crystal structure and the volume. By shifting the DFT energy eigenvalues (in our case, from WIEN2K calculations) in this way, we guarantee that when we fit the tight-binding bands to these energy eigenvalues we will reproduce the DFT total energies when summing over these eigenvalues. For the nonorthogonal tight-binding model, we use a basis consisting of s, p, and d orbitals. The NRL parametrization requires 73 parameters to describe the distance dependence of all of the s-p-d Hamiltonian and overlap matrix elements,[2–4,12] upon which the accuracy and transferability of the tight-binding method depends.

The database used for fitting the tight-binding parameters of zirconium was calculated from the energy bands and total energies of the WIEN2K full-potential LAPW codes.[13] The GGA (Ref. 1) potential was used to include the effects of exchange and correlation. To fit the 73 parameters to the DFT database, we used a standard nonlinear least-squares algorithm,[14] the Levenberg-Marquardt method. For the cubic structures, the symmetry of special $\mathbf{k}$ points in the first Brillouin zone is taken into account.[15]

Since fitting is a highly nonlinear process, it is easy to get trapped in false minima and to generate bad fits. For this reason we describe our fitting procedure, since it may help others find good tight-binding fits. Initially, we started by only fitting to the special $\mathbf{k}$ points of three cubic crystal structures (bcc, fcc, and simple cubic), at nine volumes in the
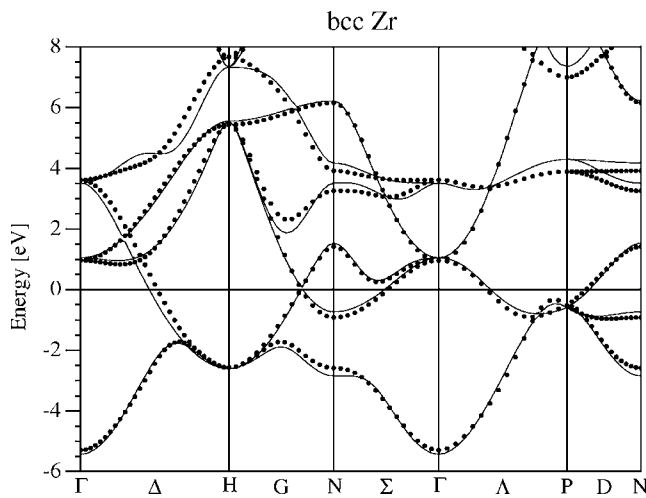
FIG. 1. Comparison of energy eigenvalues for the bcc crystal structure. The lines are the DFT results, and the dots are calculated from the fitted TB model in which only energy bands were fitted. All energies are relative to the respective Fermi energy (the zero of energy) for each method.
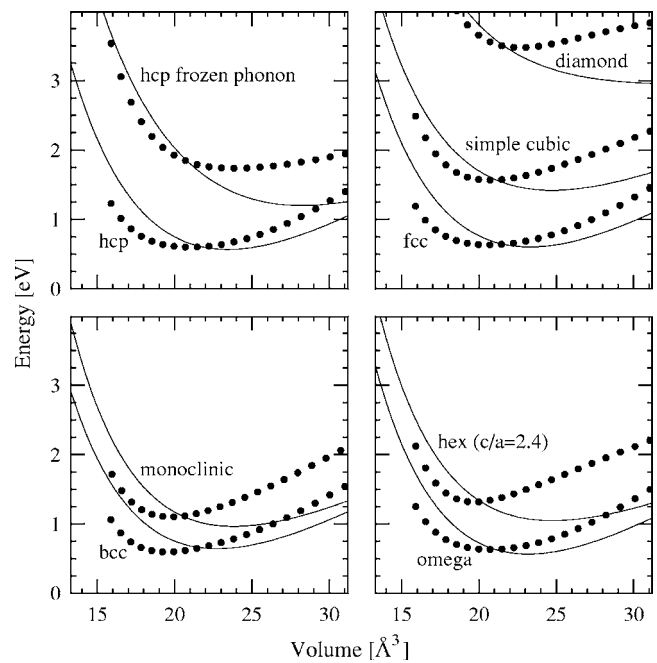

FIG. 2. Comparison of total energies for the crystal structures that are included in the tight-binding fitting database. Each total energy is normalized per atom to make it possible to compare structures with different numbers of atoms in the unit cell. The lines are the DFT results, where we fit the energies for specific volumes to the parametrization of Ref. 35, and then plot this curve, which is a highly accurate representation of the DFT energies. The dots are calculated from the TB model in which only energy bands were fitted. Since the energy is only determined to an arbitrary constant (only relative energies are meaningful), we have shifted the zero of energy to make the numbers relatively small and positive.

range from 15.7 to 30.7 Å^3/atom. It is important not to include too much information into the database when starting a fit. The symmetrized energy bands constrain the parametrization and push it towards the physically meaningful part of parameter space.[15] This is important since the optimization process easily gets trapped in a large number of local minima of the vast 73-dimensional parameter space.

Next, we added other crystal structures that seemed important to us, namely, the hcp, diamond, and ω structure, into the database, still only fitting to band energies (over the same range of volumes). It is important not to "overwhelm" the fitting procedure with too many crystal structures and constraints at once. Adding a few crystal structures at a time allows the procedure to slowly move the fit into a better part of parameter space. The tight-binding fit at this stage is shown in Figs. 1 and 2. Figure 1 shows a comparison of the DFT and the tight-binding energy bands for the bcc structure at the experimental equilibrium volume. This comparison is very representative for other crystal structures, and it shows that the tight-binding energy bands are in remarkably good agreement with DFT. At other volumes the comparison is only slightly worse. However, when looking at the total energies in Fig. 2, the agreement is less good. This mismatch might be surprising since the total energies are just a sum of the band energies. However, the errors in the structural energies in Fig. 2 are on the order of a few tenths of eV, whereas Fig. 1 shows the band-structure energy eigenvalues on a scale that is the order of 10 eV. This scale, which is necessary to show the full energy bands, can be slightly misleading with respect to the size of the errors. The errors in the energy bands can be as large as a tenth of an eV, and these errors can add up when summing over all the occupied bands throughout the Brillouin zone. Unfortunately, even after many attempts, we were not able to increase the accuracy of the tight-binding fit by only fitting to energy bands.

To increase the accuracy of the total energies, we then included the total energies themselves into the fitting DFT

database, with weights between 1000 and 5000 larger than the weights of the individual energy eigenvalues. We also included the following additional crystal structures into our database (these are related to relevant frozen phonons and elastic-constant deformations): (i) the hexagonal crystal structure with the c/a ratios of 0.8 and 2.4, and (ii) an hcp frozen phonon that corresponds to the longitudinal phonon frequency at the Γ point. Figures 3 and 4 show the comparison of DFT with the new fit to the tight-binding energy bands and total energies. The tight-binding total energies shown in Fig. 4 are now much closer to DFT. However, when looking at Fig. 3, we see that the tight-binding energy-band fit is severely degraded. This is problematic since the energy bands contain all of the important physics upon which the tight-binding method is based. If they become less accurate, there is a danger that the method will lose its physical meaning, and hence also its transferability, i.e., the ability of the method to correctly predict band and total energies for structures that are not included in the database. Nonetheless, since almost all materials and thermodynamic properties depend so heavily on the total energies, we were forced to make this trade-off and the tight-binding fit of Fig. 4 that heavily weights the total energies was used for calculating almost all materials and thermodynamic properties in this paper. To improve this situation would require either better and more flexible formulations of the tight-binding parametrization
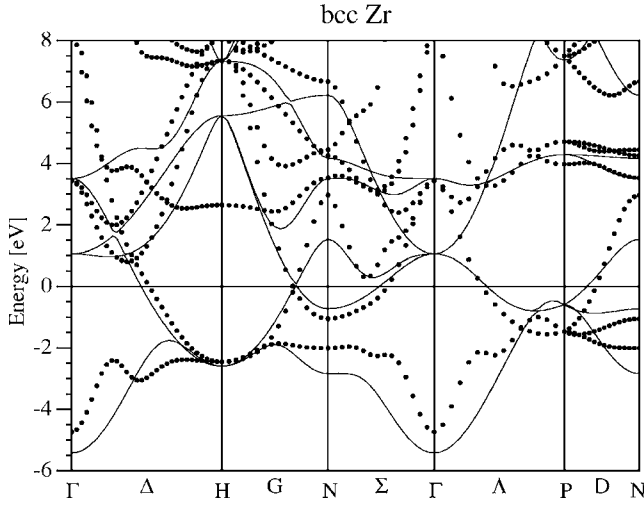
FIG. 3. Comparison of energy eigenvalues for the bcc crystal structure. The lines are the DFT results (using the parameterization from Ref. 35), and the dots are calculated from the TB model in which energy bands and total energies were fitted. All energies are relative to the respective Fermi energy (the zero of energy) for each method.

(perhaps embedded-atom-like terms for the nearest-neighbor matrix elements) or finding a more physical fit than any of the large number of nonphysical minima in which one can easily get trapped. Ideally, both the tight-binding energy bands as well as the total energies should agree extremely well with first-principles GGA-DFT band-structure calculations.

III. PHONONS

In standard textbooks (see, e.g., Chap. 22 in Ref. 16) phonon frequencies are derived from an expansion of the total energy of a solid as a function of atomic displacements. In the literature this method is called the direct-force method,[17,18] and relies on evaluating the forces on all atoms (l,k), i.e., the kth atom in lth cell, in which one atom $(0,k')$ has been displaced by a small amount away from its equilibrium position. Since there is an explicit expansion of the total energy to second order in atomic displacements, some care must be taken to make sure that these displacements are sufficiently small so that the expansion is accurate and does not implicitly include higher-order terms. In this paper we use the quasiharmonic approximation, whereby the force constants are calculated as a function of volume (i.e., the total energy is expanded as a function of displacement around the atomic positions of the perfect lattice, whose lattice constants change as a function of volume).

In the quasiharmonic approximation, the force constants are given by

$$\phi_{\alpha\beta}(0k',lk) = -\frac{\partial F_\beta(l,k)}{\partial u_\alpha(0,k')} \approx -\frac{F_\beta(l,k)}{u_\alpha(0,k')}, \qquad (2)$$

i.e., the ratio of the negative force on atom (l,k) in the β direction to the displacement of atom $(0,k')$ in the α direc-
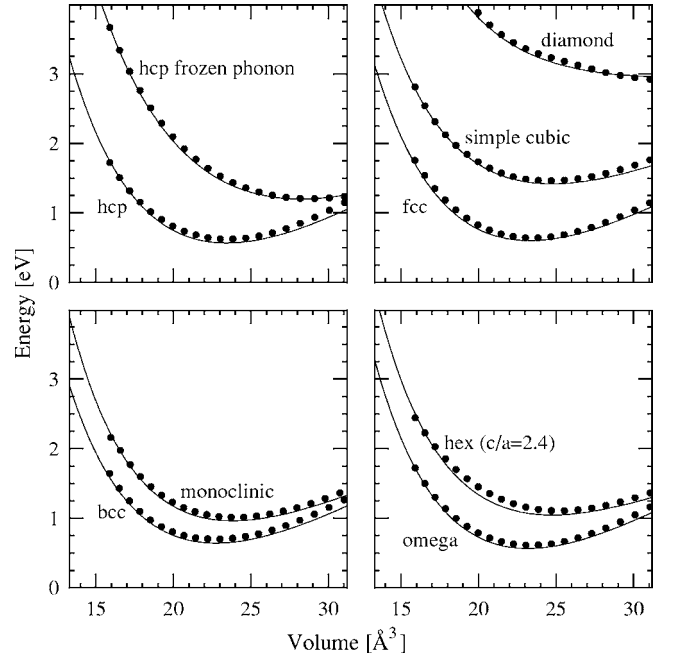

FIG. 4. Comparison of total energies for crystal structures included in the tight-binding fitting database. Each total energy is normalized per atom to make it possible to compare structures with different numbers of atoms in the unit cell. The lines are the DFT results, and the dots are calculated from the TB model in which energy bands and total energies were fitted. This fit is used for the supercell calculations and phonons. Since the energy is only determined to an arbitrary constant (only relative energies are meaningful), we shifted the zero of energy to make the numbers relatively small and positive.

tion. In the TB model, the actual calculation of the forces in Eq. (2) is achieved by evaluating analytic derivatives of the Hamiltonian and overlap matrix elements and the on-site terms.[19] Once the force constants have been calculated, the phonons are evaluated by diagonalizing the Fourier transform of the real-space dynamical matrix,

$$M_{\alpha\beta}(\mathbf{q},kk') = \sum_{l'} \phi_{\alpha\beta}(0k,l'k')\exp\{i\mathbf{q}\cdot[\mathbf{x}(l',k')-\mathbf{x}(0,k)]\},$$

$$(3)$$

where $\mathbf{q}$ is the wave vector and $\mathbf{x}(l,k)$ is the atom position.

This formula is correct for an infinitely large system. However, because our tight-binding calculations are done with periodic boundary conditions, we are forced to evaluate this equation within a supercell. Because of the computational limitations of diagonalizing a large number of atoms, our supercell size is limited. In this case, if the forces do not vanish inside the supercell, errors due to (super)cell-cell interactions are introduced.[18] Also, the supercell, which consists of replicas of the primitive or conventional unit cell, does in general not have the right crystal symmetry. Therefore cell-cell interactions will contribute force constants that violate symmetry rules.

Since our goal is to calculate the best approximation possible to the infinite crystal limit for the real-space dynamical

matrix, we have to apply corrections to our periodic super-cell results to obtain this. The most important correction is to first restore the correct symmetry. If we consider the effect of symmetry operators on the dynamical matrix, then for the space-group element $\hat{S}_m$, where $\mathbf{S}$ is its proper or improper rotation and $\mathbf{v}$ is its translation, we have that

$$\hat{S}_m\mathbf{x}(l,k) = \mathbf{x}(L,K) = \mathbf{S}_m\mathbf{x}(l,k) + \mathbf{v}_m. \tag{4}$$

Since the total energy of a system cannot change under a symmetry operation, if this symmetry is imposed on the system and one compares like terms in the expansion, the following symmetry relation is obtained (see pp. 28–29 of Ref. [20]):

$$\phi_{\alpha\beta}(lk,l'k') = \mathbf{S}_m\phi_{\alpha\beta}(lk,l'k')\mathbf{S}_m^T, \tag{5}$$

where ϕ is a 3×3 matrix with elements $\phi_{\alpha\beta}$ (see Ref. [20]) and the superscript T implies transposition. Since Eq. (5) will no longer hold when cell-cell interactions are present, it is necessary to restore this symmetry so that our calculated phonons will have the correct symmetry, such that the eigenvalues of Eq. (3) are unchanged by $\mathbf{q}\rightarrow\mathbf{Sq}$. We achieve this by applying all symmetry operations, and then averaging over these within Eq. (5). This involves replacing each force constant

$$\phi_{\alpha\beta}(0k,l'k')\exp\{i\mathbf{q}\cdot[\mathbf{x}(l',k')-\mathbf{x}(0,k)]\} \tag{6}$$

in Eq. (3) by

$$\frac{1}{N}\sum_{m=1}^{N}\mathbf{S}_m\phi_{\alpha\beta}(0k,l'k')\mathbf{S}_m^T\exp\{i\mathbf{q}\cdot S_m[\mathbf{x}(l',k')-\mathbf{x}(0,k)]\}, \tag{7}$$

where N is the number of space-group elements. In our calculation of the dynamical matrix, Eq. (3), we then sum over all primitive cells in the supercell. The hope is that the calculations will converge for a sufficiently large supercell size.

We should note that this scheme differs somewhat from the original direct-force method,[18] where the dynamical matrix was summed over shells of nearest-neighbor force constants, and was truncated after the fifth shell for the alkali metals. In our calculations, the sum over shells of nearest-neighbor force constants did not converge, and truncating this sum over shells led to a violation of the sum rule,

$$\sum_{l'k'}\phi_{\alpha\beta}(0k,l'k') = 0. \tag{8}$$

When this equation does not hold, the acoustical branches of the phonon spectrum do not go to zero as q goes to zero, as they should. Using the symmetrized form of the force constants and summing over all primitive cells in the supercell restored this sum rule in our calculations.

Using this scheme, we have calculated the phonon energies from force constants evaluated from three different supercells, as shown in Fig. 5. These test calculations were done at the theoretical equilibrium. Here, the evaluation of the dynamical matrix, Eq. (3), included only atoms in primitive cells included in the supercell. Along each primitive vector, the primitive cells of the supercell were chosen sym-
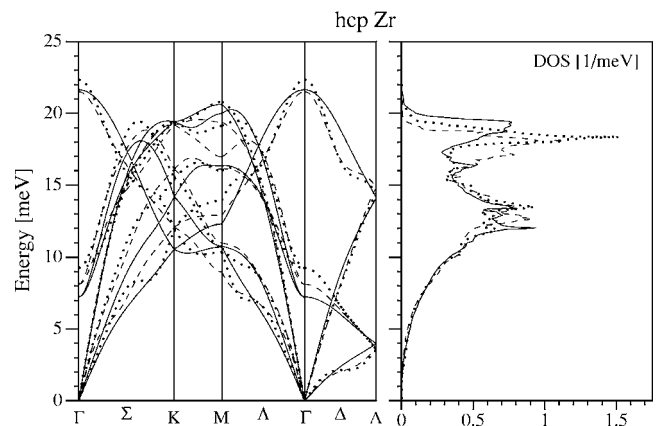

FIG. 5. The hcp phonon energy band structure obtained from $3\times3\times3$ (solid), $4\times4\times4$ (dashed), and $5\times5\times4$ (dotted) supercells.

metrically around the origin. In cases where a supercell has an even number of primitive cells along one direction, one cell was duplicated (with adjusted weight) and transposed by the corresponding basis vector of the supercell, such that primitive cells are symmetrical around the origin. It should be emphasized that the phonons depend on very small differences in the total energy of the tight-binding calculations.

In this figure, the phonon energies are reasonably converged with respect to the supercell size. The effect of larger supercell size does not seem to change the overall spectrum by very much, but does appear to introduce some oscillating behavior in the phonon dispersion curves that is unphysical. These oscillations are probably errors introduced by adding additional Fourier components into the phonon spectrum; it is likely that these are incorrectly calculated due to supercell-supercell interactions, and the associated necessity of applying the symmetry operations to the force constants [cf. Eq. (5)]. Hence we believe that our most reliable spectrum is actually the $3\times3\times3$, which does not have these spurious oscillations. Note that the largest differences in the overall phonon density of states (right-hand side of Fig. 5) is for the highest phonon frequencies.

In Fig. 6 we show a comparison of this $3\times3\times3$ supercell calculation with experimental phonons at room temperature.[7] The overall shape of the theoretically calculated spectrum qualitatively agrees with the experimental spectrum. This rough agreement with experiment suggests that we are picking up the dominant part of the dynamical matrix with the short-range part of the force constants; it is the last 20% that is hard to converge due to the long-range forces. The two main differences between the theoretical and experimental spectrum are (i) the overall theoretical dispersion curves are on average about 20% too low, and (ii) the lowest acoustic-phonon branches are too soft. Although our calculations are done for zero temperature, the experimental temperature dependence[7] of the phonon dispersion curves between 5.5 and 1007 K suggest that our errors are larger than differences between the 5.5-K and room-temperature spectrum (some modes increase and others decrease as a function of temperature). Unfortunately, the 5.5-K published data are very sparse, which is why we plotted the experimental room-temperature curves in Fig. 6.
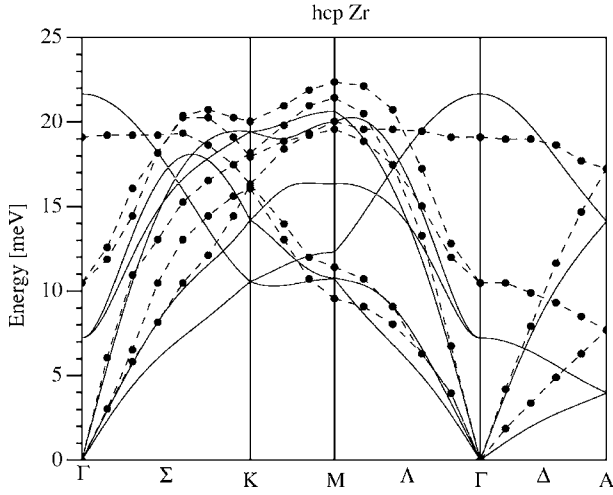
FIG. 6. The hcp phonon energy band structure. The solid lines show the phonon frequencies from our tight-binding calculation, using the $3 \times 3 \times 3$ supercell, the dots and dashed lines show the experimental phonon frequencies from neutron scattering at 295 K (Ref. 7).

When compared with previous tight-binding calculations for Cu metal[2] and Ti metal,[3] the agreement of the phonon spectrum with experiment is far worse for Zr. We believe that the largest errors in the phonon frequencies are attributable to the anomalously long-range behavior of the force constants, which we discuss in greater detail in Sec. VII. The long-range behavior of Zr is far more severe than for Cu or Ti, which is likely a very large reason for the greater discrepancies with experiment. It should be noted, however, that even for Cu and Ti, there appears to be a slight systematic underestimate of the highest phonon frequencies, which may also indicate some smaller previously unsuspected convergence problems for these systems as well. Finally, the lowest branches of the acoustic-phonon spectrum for Cu and Ti are in good agreement with experiment while that for Zr is poor. Since the small wave-vector behavior of the phonons is directly proportional to the sound velocities of the crystal in different directions, which only depend on the elastic constants, we have therefore calculated the elastic constants and sound speeds for Zr with our tight-binding model, and present these results in the next two sections.

Despite these problems, thermodynamic properties (particularly at higher temperatures when many phonon modes are sampled) often average over the phonon spectrum and are less sensitive to the level of errors we have presented above. We have recently been able to use the computational efficiency of our TB model to provide a reasonably accurate prediction[4] for the hcp-to-ω and the ω-to-bcc Zr phase-transition phase boundaries over a moderate temperature range. However, this paper is the first time we have provided the full details and problems associated with the tight-binding fits and the method used for calculating the phonon frequencies.

IV. ELASTIC CONSTANTS

As discussed above, the elastic constants determine the sound speeds in different directions in a crystal, which, in turn, give the slope (ω/q) of phonon-dispersion curves for small wave vectors (q). The elastic constants therefore serve as an important check on the quality of phonon calculations as well as being themselves an important physical parameter for a material.

Usually, the treatment of elasticity is given for a crystal free of stress. Since we are interested in calculations for hexagonal crystals for arbitrary c/a, this situation will not hold for us. We therefore write down the general case first and then specialize to stress-free crystals.

A linear deformation of the lattice is expressed by multiplying the Bravais matrix **a**, which contains the three Bravais vectors in its columns, with a deformation matrix

$$\mathbf{e} = \begin{pmatrix} 1 + u_{xx} & u_{xy} & u_{xz} \\ u_{yx} & 1 + u_{yy} & u_{yz} \\ u_{zx} & u_{zy} & 1 + u_{zz} \end{pmatrix}. \qquad (9)$$

The Taylor expansion of the total-energy density due to the deformation has the form

$$E(\mathbf{e}) = E(0) + \sum_{\alpha\beta} \tau_{\alpha\beta} u_{\alpha\beta} + \frac{1}{2} \sum_{\alpha\beta\gamma\lambda} S_{\alpha\beta,\gamma\lambda} u_{\alpha\beta} u_{\gamma\lambda} + \cdots, \qquad (10)$$

where $S_{\alpha\beta,\gamma\lambda}$ is symmetric in $(\alpha\beta, \gamma\lambda)$, i.e.,

$$S_{\alpha\beta,\gamma\lambda} = S_{\gamma\lambda,\alpha\beta}. \qquad (11)$$

We assume the stress matrix $\tau_{\alpha\beta}$ to be present in the unstrained material, i.e., even before applying the deformation matrix. Rigidly rotating the strained crystal must leave the energy density invariant. As shown in Ref. 21, this invariance requires

$$\tau_{\alpha\beta} = \tau_{\beta\alpha}, \qquad (12)$$

and

$$\tau_{\alpha\lambda}\delta_{\beta\gamma} - \tau_{\beta\lambda}\delta_{\gamma\alpha} + S_{\alpha\beta,\gamma\lambda} - S_{\beta\alpha,\gamma\lambda} = 0. \qquad (13)$$

In order to evaluate the stress matrix $\tau_{\alpha\beta}$ and Huang's coefficients $S_{\alpha\beta,\gamma\lambda}$, we first apply strain matrices of the form

$$u_{\eta\rho} = \delta_{\alpha\eta}\delta_{\beta\rho} u, \qquad (14)$$

i.e., only the strain component $u_{\alpha\beta}$ equals u, all other strain components equal zero. There are nine matrices of this form, corresponding to the nine different choices of α and β. Inserting Eq. (14) into Eq. (10) gives

$$E(\mathbf{u}) = E(0) + \tau_{\alpha\beta} u + \frac{1}{2} S_{\alpha\beta,\alpha\beta} u^2. \qquad (15)$$

Calculating $E(u)$ for all choices of α and β, and estimating the first and second derivatives from polynomial fits, we can calculate all the stresses $\tau_{\alpha\beta}$ and Huang's coefficients of the form $S_{\alpha\beta,\alpha\beta}$ directly. Next, we apply strain matrices of the form

$$u_{\eta\rho} = (\delta_{\alpha\eta}\delta_{\beta\rho} - \delta_{\gamma\eta}\delta_{\lambda\rho}) u \quad (\alpha,\beta \neq \gamma,\lambda), \qquad (16)$$

i.e., only the two strain components $u_{\alpha\beta}$ and $u_{\gamma\lambda}$ are nonzero and opposite in sign. There are 36 strain matrices of this form, which corresponds to selecting two out of nine elements. Inserting Eq. (16) into Eq. (10) gives

TABLE I. Elastic constants in GPa for the hcp structure. The experimental values in the first column (Expt.) are from Ref. 36. The second column shows DFT results from Ref. 24 at their theoretical equilibrium. Note that these calculations were done for conventional LDA and not for GGA; LDA tends to overbind transition metals and the volume is reduced when compared to experiment. This causes about a 20% over-estimate for the bulk modulus (Ref. 24) and one expects the other LDA elastic constants to similarly be somewhat too large. The remaining columns show the elastic constants calculated from the TB model. In the third and fourth columns (TB-E, TB-T), the elastic constants were evaluated by direct distortion of the unit cell (cf. Sec. IV) at the experimental and theoretical equilibrium volumes, respectively. Note that the theoretical equilibrium volume minimized the total energy and does not contain any zero-point motion effects. The last three columns show the elastic constants evaluated through the Born and Huang relations at theoretical equilibrium for different supercell sizes, Sec. VI.

	Expt.	DFT	TB-E	TB-T	$3\times3\times3$	$4\times4\times4$	$5\times5\times4$
C_{11}	144	156	133	142	120	121	130
C_{12}	74	65	80	71	61	18	−8
C_{13}	67	76	73	71	48	32	65
C_{33}	166	182	148	147	169	164	152
C_{44}	33	25	7	8	19	44	25
τ_{xx}, τ_{yy}		0	−0.6	0	3.5	14.5	1.0
τ_{zz}		0	−2.0	0	−7.0	−29.0	−2.0
$V/\text{Å}^3$	23.34	22.19	23.34	23.58	23.58	23.58	23.58
c/a	1.593	1.583	1.593	1.625	1.625	1.625	1.625

$$E(\mathbf{u}) = E(0) + (\tau_{\alpha\beta} - \tau_{\gamma\lambda})u + \left(\tfrac{1}{2}S_{\alpha\beta,\alpha\beta} - S_{\alpha\beta,\gamma\lambda} + \tfrac{1}{2}S_{\gamma\lambda,\gamma\lambda}\right)u^2, \tag{17}$$

where we have used Eq. (11). Since we have already evaluated the terms $S_{\alpha\beta,\alpha\beta}$, we are now in a position to calculate all the coefficients $S_{\alpha\beta,\gamma\lambda}$ from polynomial fits. It is important to note that the procedure outlined above does not assume the crystal to be stress free, nor does it assume the symmetry of any crystal class.

Since the tight-binding method is computationally inexpensive, we have calculated all the 45 energy-strain curves for both the experimental ($V=23.34$ Å^3/atom, $c/a=1.593$) and theoretical ($V=23.58$ Å^3/atom, $c/a=1.625$) equilibrium. For each type of strain, we have chosen five values for u of ±0.01, ±0.005, and zero. We have also carefully checked the convergence of $S_{\alpha\beta,\gamma\lambda}$ as a function of the number of k points used, and found that 40^3 k points are sufficient to converge the coefficients to an accuracy of 0.25 GPa.

While the coefficients $S_{\alpha\beta,\gamma\lambda}$ are conveniently determined from Eq. (10), they lack symmetry in (α,β) and (γ,λ). Only if the stress matrices $\tau_{\alpha\beta}$ vanish does Eq. (13) reduce to $S_{\alpha\beta,\gamma\lambda}=S_{\beta\alpha,\gamma\lambda}$. Using Eq. (11), we see that both pairs of indices are then symmetric. This allows the use of the customary simplifying Voigt notation that contracts pairs of indices into single indices,[20,22] i.e., $xx\to1$, $yy\to2$, $zz\to3$, $(yz,zy)\to4$, $(xz,zx)\to5$, and $(xy,yx)\to6$.

It is therefore convenient to introduce elastic constants $C_{\alpha\beta,\gamma\lambda}$ which have the full symmetry

$$C_{\alpha\beta,\gamma\lambda} = C_{\beta\alpha,\gamma\lambda} = C_{\alpha\beta,\lambda\gamma} = C_{\gamma\lambda,\alpha\beta}. \tag{18}$$

By means of Eq. (13), we see that this is achieved by defining

$$C_{\alpha\beta,\gamma\lambda} = S_{\alpha\beta,\gamma\lambda} - \tau_{\beta\lambda}\delta_{\alpha\gamma}. \tag{19}$$

In fact, these elastic constants $C_{\alpha\beta,\gamma\lambda}$ are obtained by expanding the energy density in terms of finite strain parameters $\eta_{\alpha\beta}=\tfrac{1}{2}(u_{\alpha\beta}+u_{\beta\alpha}+\sum_\gamma u_{\gamma\alpha}u_{\gamma\beta})$ instead of the deformation parameters $u_{\alpha\beta}$ themselves.[23]

We are now in a position to state our results for both the experimental and theoretical equilibrium in terms of the elastic constants C_{ij} using the Voigt notation. These results reveal relations among the elastic constants C_{ij}, which are specific for every crystal class (see, e.g., Table 9 in Ref. 22). Since our concern is a hexagonal crystal, only the five independent elastic constants C_{11}, C_{12}, C_{13}, C_{33}, and C_{44} are shown in Table I. The columns labeled TB and Expt. in Table I show the results of the tight-binding calculations and experimental results for the elastic constants for the hcp structure. For the tight-binding calculation performed at the experimental equilibrium volume, we find an anisotropic stress of $\tau_{xx}=\tau_{yy}=-0.6$ GPa and $\tau_{zz}=-2.0$ GPa. For the tight-binding calculation performed at the theoretical equilibrium, we find the τ's to be vanishing within numerical error, as one would expect. The column labeled DFT was taken from the first-principles calculations given in Ref. 24. The best theoretical calculations (DFT) give C_{11}, C_{12}, C_{13}, and C_{33} within $8-13$ % of experiment; however, C_{44} is 24% too small. The direct TB calculations (labeled TB) for C_{11}, C_{12}, C_{13}, and C_{33} are within $6-10$ % of experiment; however, C_{44} is much too small, being about 1/4 of the experimental value. Thus for four of the five elastic constants tight binding is as accurate as first-principles DFT calculations. The main discrepancy is for C_{44}, which is also problematic for DFT.

In Table I we also present results for the elastic constants that depend on long-wavelength expansions of the phonon

TABLE II. Calculated sound speeds in km/s for the hcp structure. The first panel shows the sound speeds in the xy plane (this includes the Γ to K and the Γ to M directions in the phonon dispersion curves), and the second panel shows the sound speeds in the z direction (this is the Γ to A direction). For the geometries that we used, all sound speeds in the xy plane are independent of direction. The column headings are the same as in Table I. The sound speeds were calculated from either the relevant elastic constants or the $S_{\alpha\beta,\gamma\lambda}$ matrices.

		Expt.	DFT	TB-E	TB-T	$3\times3\times3$	$4\times4\times4$	$5\times5\times4$
xy	c_1	2.25	1.96	0.98	1.13	1.87	3.02	2.00
xy	c_2	2.32	2.65	2.00	2.37	2.28	3.20	3.30
xy	c_3	4.71	4.90	4.52	4.69	4.39	4.60	4.51
z	$c_{1,2}$	2.25	1.96	0.86	1.12	1.36	1.54	1.88
z	c_3	5.06	5.30	4.75	4.78	5.02	4.58	4.84
	$V/\text{Å}^3$	23.34	22.19	23.34	23.58	23.58	23.58	23.58
	c/a	1.593	1.583	1.593	1.625	1.625	1.625	1.625

dynamical matrix (Born and Huang relations), which will be discussed further in Sec. VI. The TB calculations using the Born and Huang relations for the different supercell sizes fluctuate and have clearly not converged. The implications of these errors for the phonon calculations will be presented in Sec. VI. It should be noted that the phonon spectrum has some temperature dependence,[7] which is also true for the elastic constants. The experimental elastic constants were determined at room temperature.

V. SOUND VELOCITIES

The sound speeds along any direction in the arbitrarily stressed crystal can be calculated from the elastic equations of motion,[23]

$$\rho\frac{\partial^2 u_\alpha}{\partial t^2} = \sum_{\gamma\beta\lambda} S_{\alpha\gamma,\beta\lambda}\frac{\partial^2 u_\beta}{\partial x_\lambda \,\partial x_\gamma}, \tag{20}$$

where ρ is the density. This equation describes the movement of elastic disturbances through a homogeneous continuous media. As usual, a plane-wave solution for Eq. (20) is assumed and requires solving the eigenvalue problem

$$\rho\omega^2(\mathbf{q})\mathbf{u}(\mathbf{q}) = \mathbf{A}(\mathbf{q})\mathbf{u}(\mathbf{q}), \tag{21}$$

where the real symmetric matrix $\mathbf{A}$ is given by

$$A_{\alpha\beta}(\mathbf{q}) = \sum_{\gamma\lambda} S_{\alpha\gamma,\beta\lambda}q_\gamma q_\lambda. \tag{22}$$

Notice that since $\mathbf{A}(\mathbf{q})$ is quadratic in $\mathbf{q}$, $\omega^2(\mathbf{q})$ will be as well, and therefore $\omega(\mathbf{q})$ will be linear in q, i.e., $\omega(\mathbf{q})=c(\hat{\mathbf{q}})q$ where $c(\hat{\mathbf{q}})$ are the sound velocities of the acoustic waves in the direction $\hat{\mathbf{q}}=\mathbf{q}/q$.

If the crystal is unstressed, from Eq. (19) one obtains $C_{\alpha\beta,\gamma\lambda}=S_{\alpha\beta,\gamma\lambda}$. Using the Voigt notation, one can show from the symmetry among the constants C_{ij} for a hexagonal media[22] that Eq. (22) becomes

$$A_{xx} = C_{11}q_x^2 + (C_{11} - C_{12})/2q_y^2 + C_{44}q_z^2,$$

$$A_{yy} = (C_{11} - C_{12})/2q_x^2 + C_{11}q_y^2 + C_{44}q_z^2,$$

$$A_{zz} = C_{44}(q_x^2 + q_y^2) + C_{33}q_z^2,$$

$$A_{yz} = (C_{13} + C_{44})q_y q_z,$$

$$A_{xz} = (C_{13} + C_{44})q_z q_x,$$

$$A_{xy} = (C_{11} + C_{12})/2q_x q_y. \tag{23}$$

An interesting consequence is that the three velocities along any direction in the xy plane, i.e., $\hat{q}_x=\cos(\varphi)$, $\hat{q}_y=\sin(\varphi)$, and $\hat{q}_z=0$, are independent of the angle φ for hexagonal symmetry. In this plane,

$$c_1 = \sqrt{C_{11}/\rho}, \quad c_2 = \sqrt{(C_{11} - C_{12})/2\rho}, \quad c_3 = \sqrt{C_{44}/\rho}. \tag{24}$$

Along the z direction ($\hat{q}_z=1$, $\hat{q}_x=\hat{q}_y=0$), one obtains

$$c_{1,2} = \sqrt{C_{44}/\rho}, \quad c_3 = \sqrt{C_{33}/\rho}. \tag{25}$$

Especially if the sound velocities depend on differences of elastic constants, sound speeds can be very sensitive to small changes in the elastic constants. Since the sound speeds correspond to the small-wavelength behavior of the acoustic phonons, a good prediction of the elastic constants from the TB model is important for the model to correctly calculate low-q phonons.

In Table II we present our calculations for the sound speeds. The experimental, DFT, and TB-T sound speeds were calculated from the elastic constants presented in Table I and Eqs. (24) and (25). The TB-E and supercell calculations used the relevant $S_{\alpha\beta,\gamma\lambda}$ matrices and diagonalized the sound-speed equations (21) and (22). The effects of the anomalously low value for C_{44} in the tight-binding calculations lead to very low sounds for c_1 in the x-y plane and $c_{1,2}$ in the z direction, and, in turn, explain the soft lowest acoustic branch in the theoretically calculated phonon spectrum (see Fig. 6). The other sound speeds, which depend more on the other elastic constants, are in relatively good agreement with experiment. The supercell calculations are derived from the phonon force constants, and are discussed in Sec. VI.

VI. BORN AND HUANG RELATIONS

Born and Huang[25] demonstrated the connection between the elastic constants and the force constants for a crystal in equilibrium. These relations are obtained by expanding Eq. (3) in the long-wavelength limit (small $\mathbf{q}$), and comparing the three acoustic branches to the solutions of the elastic equations that involve elastic restoring vibrations and that are governed by the elastic constants. For the case of a crystal with inversion symmetry the relations assume a simpler form. For small $|\mathbf{q}|$, the dynamical matrix can then be expanded as (see also Refs. 20 and 21)

$$M(\mathbf{q}) = M^{(0)} + \frac{1}{2} \sum_{\gamma\lambda} M^{(2)}_{\gamma\lambda} q_\gamma q_\lambda + \cdots . \qquad (26)$$

The elements of the matrices are given by

$$M^{(0)}_{\alpha\beta}(kk') = \sum_{l'} \phi_{\alpha\beta}(0k, l'k') \qquad (27)$$

and

$$M^{(2)}_{\alpha\beta,\gamma\lambda}(kk') = -\sum_{l'} \phi_{\alpha\beta}(0k, l'k') x_\gamma(0k, l'k') x_\lambda(0k, l'k'), \qquad (28)$$

where

$$x_\gamma(0k, l'k') = x_\gamma(0, k) - x_\gamma(l', k'). \qquad (29)$$

The elastic constants can then be calculated from

$$C_{\alpha\gamma,\beta\lambda} = [\alpha\beta, \gamma\lambda] + [\beta\gamma, \alpha\lambda] - [\beta\lambda, \alpha\gamma], \qquad (30)$$

where the square brackets are defined as (v is the volume of the primitive cell)

$$[\alpha\beta, \gamma\lambda] = \frac{1}{2v} \sum_{kk'} M^{(2)}_{\alpha\beta,\gamma\lambda}(kk'). \qquad (31)$$

As noted above, these equations are only valid for a crystal in equilibrium. They can, however, be generalized to the case of anisotropic stresses. Huang[21] has made this generalization, and it turns out that only the average pressure p is not expressible in the general theory. Huang's coefficients, which are defined by

$$S_{\alpha\gamma,\beta\lambda} = [\alpha\beta, \gamma\lambda] + [\beta\gamma, \alpha\lambda] - [\beta\lambda, \alpha\gamma] + x_{\alpha\beta,\gamma\lambda}, \quad (32)$$

and are the same which appear in the elastic equations of motion (20), introduce the coefficients $x_{\alpha\beta,\gamma\lambda}$. These new coefficients $x_{\alpha\beta,\gamma\lambda}$, as well as the stresses $\tau_{\alpha\beta}$, are completely expressible in terms of the square brackets and the average pressure. Since these relations are somewhat lengthy, we refer the interested reader to Ref. 21. Again, $S_{\alpha\gamma,\beta\lambda}$ will (in general) lack the symmetry (18) but we can use Eq. (19) to state our results using the Voigt notation. Therefore it is possible to evaluate elastic constants by two completely independent methods: (i) by the use of the above Huang relations from the force constants, and (ii) by directly applying various strains to the crystal (Sec. IV).

For the different supercells, which were used to create Fig. 5, we applied the Born and Huang relations and calculated the elastic constants. These results are shown in Table I. Even though the phonons themselves (Fig. 5) are reasonably converged, the resulting elastic constants are not converged. These elastic constants should converge to the entries in column TB-T. The Born-Huang relations emphasize the long-range force constants, since Eq. (28) is quadratic in distance. In order to converge the elastic constants that are obtained from Eq. (30), the force constants need to decay more rapidly than x^{-2} with distance. The poor convergence of the elastic constants, obtained from the different supercells in Table I, are an indication of long-ranged force constants. In addition, even though the supercell calculations were carried out at the theoretical equilibrium volume, we see that the stresses obtained from the force constants are not vanishing. They appear to be getting smaller with increasing supercell size, however. We will discuss this issue in the following section.

The sound speeds that are calculated from the Born and Huang relations are shown in Table II. These give the slope of the phonon dispersion curves at small q. The deviation from the experimental phonons due to differences in these sound speeds with respect to experiment for the $3 \times 3 \times 3$ supercell can clearly be seen in the small-q differences seen in Fig. 6. For a consistent theory, the sound speeds for the supercells should converge to those in column TB-T. The Born and Huang relations are a sensitive test of the supercell convergence of phonons calculated by the direct-force method.

VII. LONG-RANGE FORCES

In order to understand the range of the force constants at a large distance, we have chosen a $1 \times 1 \times 25$ hcp supercell that stretches along the z direction. By displacing one atom in this supercell in the z direction, we actually displace a layer of atoms. The resulting force on every atom is called a planar force, which is, however, proportional to the force that would result if only one atom in the plane were displaced.[26] Figure 7 shows these forces and, from linear regression, we find the decay to be approximately $z^{-1.48}$. To verify this result and to test whether it was associated with the TB model or was an inherent feature in the physics of this material, we have also done the same calculation using the VASP first-principles code[27] and employing GGA.[1] The result of this calculation is also shown in Fig. 7. Here, we find the decay to be even longer ranged, with a falloff of approximately $z^{-0.94}$.

This explains why the elastic constants, which are obtained from the Born and Huang relations, Eq. (30), could not be converged. Many applications of this supercell approach have been applied to semiconductors, were the force constants are short ranged[17,26,28] (exponential) due to a finite-energy gap. In order to verify if the long-range problem is unique to zirconium, we have performed this same calculation for some other available tight-binding fits. Table III summarizes these results. We have assumed experimental volume and c/a ratios[16] for hcp Ti, Zr, and Hf. The fcc materials Al and Cu where also treated as hcp with an "ideal" $c/a = \sqrt{8/3}$ ratio, corresponding only to a staking fault. If the
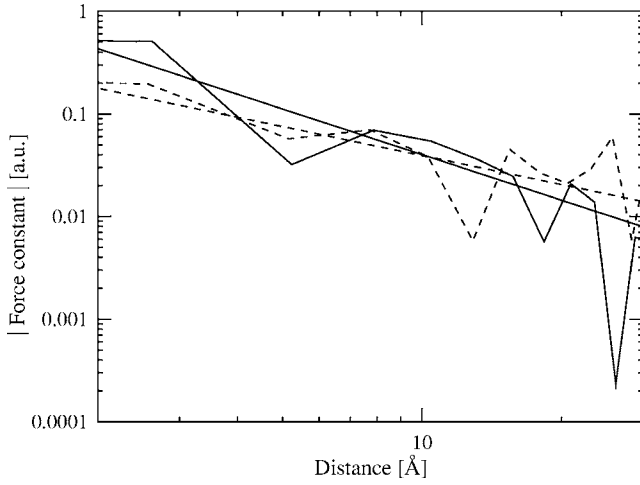
FIG. 7. The jagged solid line shows the z component of the planar force constants (from our TB model) in a $1 \times 1 \times 25$ hcp supercell, containing 50 planes of atoms along the z direction, and the straight solid line indicates the $z^{-1.48}$ decay. The dashed lines show the corresponding results from first-principles WIEN2K calculations; the straight dashed line indicates the $z^{-0.94}$ decay.

distance dependence does not fall off faster than z^{-2}, the Born-Huang relations will not converge. Although this appears to be the case for Zr, it should be noted that there is a great deal of scatter and numerical noise in the Zr distance dependence and it is probably very likely that Zr will eventually converge if an extremely large supercell is used.

With respect to zirconium, we found that increasing the size of the supercell had the largest effect on the acoustic branches near the Γ point. This is not surprising since increasing the size of the supercell mostly affects the long-range force constants, due to cell-cell interactions. In view of Eq. (3), the long-range force constants correspond to the small **q** limit, which is also the limit in which Born and Huang relations are derived. Thus increasing the supercell size has a large impact on the elastic constants, and they could not be converged.

VIII. HEAT CAPACITY

From the phonon density of states $g(\omega)$, we can calculate the lattice contribution to the specific heat[29] as

TABLE III. Decay of planar forces from the tight-binding model from $1 \times 1 \times 25$ supercell calculations within the hcp structure. The force is assumed to decay as z^p (see text). We have assumed experimental volume and c/a ratios (Ref. 16), except for the fcc materials Al and Cu where we have assumed the "ideal" c/a ratio.

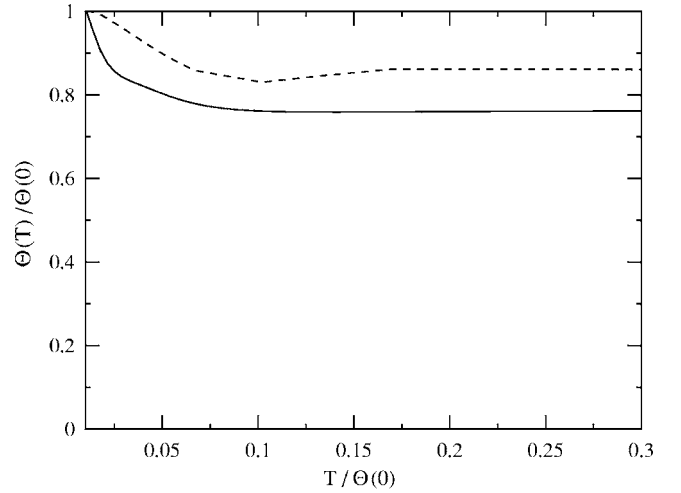| Element	Ref.	p
Al	37	−2.96
Cu	2	−4.01
Ti	3	−2.86
Hf	12	−4.18
Zr	12	−1.43
Zr	This work	−1.48

FIG. 8. Comparison of the lattice specific heat for the hcp structure in terms of an effective Debye temperature as a function of temperature (see text). The dashed line is the experimental data of Ref. 30. To get the lattice component, we have fitted the data to a curve of C_v/T vs T^2 to get the low-temperature linear electronic specific-heat component, which was then subtracted from the total specific heat. The solid curve is calculated from thermally occupying the quasiharmonic phonon frequencies from our tight-binding calculations. The results are scaled by the zero-temperature limit of the Debye temperature, which is 280.2 K for the tight-binding results and 294.0 K for the experimental results.

$$C_v^{(l)} = k \int_0^\infty \frac{\exp(\beta \hbar \omega)}{[\exp(\beta \hbar \omega) - 1]^2} (\beta \hbar \omega) g(\omega) d\omega. \quad (33)$$

However, to compare to experiment, it is typical to replot the specific-heat data as an effective Debye temperature (Θ_D) as a function of temperature. This conversion is done inverting the equation[16]

$$C_v^{(l)} = 9nk_B \left(\frac{T}{\Theta_D} \right)^3 \int_0^{\Theta_D/T} \frac{x^4 e^x dx}{(e^x - 1)^2} \quad (34)$$

in order to determine $\Theta_D(T)$, where n is the number of atoms per unit volume. A comparison of the theoretical lattice specific heat with the experimental specific heat[30,31] in terms of the Debye temperature is shown in Fig. 8. The main difference between the two is that the tight-binding Debye temperatures are about 10% below the experimental values. This is due to a thermal population of the lower acoustic branches, which are depressed in the theoretical predictions due to the anomalously small value of C_{44}.

IX. CONCLUSIONS

In this paper, we have investigated a tight-binding model for zirconium. We have been able to make a reasonably good fit of the model to first-principles calculations of the individual electronic-structure energy bands for a very wide range of crystal structures and volumes. Unfortunately, the total energies, which are just a sum over the occupied band energies, seem extremely sensitive to small errors in the band

energies and are in poor agreement with first-principles results. By also including the *ab initio* total energies into our fit (with a high weighting factor), which is the standard procedure in the literature,[2,3,12,15,32,33] the total energies for a wide variety of crystal structures and volumes are then in excellent agreement with first-principles calculations, but the comparison with the energy bands worsens. We believe that increasing the accuracy and transferability of the tight-binding fit would be greatly enhanced if the energy bands themselves could also be fit well simultaneously with the total energies. This could be achieved by either improving (i) the functional form of the tight-binding parameters, or (ii) the optimization procedure, or both. We are currently examining this issue.

We have used a tight-binding model to calculate the phonon spectrum for Zr by using the direct-force method. The results are qualitatively similar to experiment and are quantitatively adequate for thermodynamic averages over the phonon spectrum.[4] However, the highest frequency part of the spectrum appears about 20% too small, and the lowest acoustic branches are significantly lowered. Since the small-q slope of the acoustic branches are proportional to the sound speeds, which depend only on the elastic constants, we have also calculated the elastic constants for Zr. To do this we had to evaluate them using a procedure for crystals with anisotropic stress, since the theoretical minimum of the total energy is at a slightly different volume from that used for the experimental results. These techniques are useful for theoretical calculations on hexagonal and other lower symmetry crystal systems, and, in particular, for calculating elastic constants for arbitrary c/a for hexagonal crystals. We found that four of the five elastic constants are in good agreement with experiment. However, the C_{44} elastic constant is anomalously low and is responsible for the reduced sound speeds and lowered acoustic branches in the phonon spectrum. We tried to force our tight-binding fits to increase this elastic constant by adding additional distorted structures that mimic the effects of C_{44} into our tight-binding fits, but were unable to do this without destroying the otherwise excellent fits for all the other structures.

Aside from the small-q behavior, because the dominant part of the phonon spectrum is probably accounted for fairly well by the short-range behavior of the force constants, our phonons are roughly in agreement with experiment. We attribute the other errors in our calculated phonon spectrum to an unusually long-range behavior in the falloff of the force constants with distance, which require us to use symmetry corrections that in themselves may also introduce errors into the spectrum. We believe that this slow decay of atomic forces is the probable cause of the many anomalous and strongly anharmonic features of real Zr metal.

We have also estimated the decay of atomic forces with distance for other metals, and believe that their slow falloff may cause problems with using direct-force methods for many of these materials (metals often tend to have power-law behaviors for the distance dependence of many properties). This behavior was found not only for our tight-binding model but also from first-principles calculations as well. This suggests that linear-response methods[34] might be preferable for many metals; semiconductors and neutral insulators tend to have a short-ranged exponential distance dependence for which the direct-force method would be probably be more appropriate. It should be noted that the Born and Huang relations (cf. Sec. VI) are a sensitive test of the supercell convergence of phonons calculated by the direct-force method.

ACKNOWLEDGMENTS

[1] J. P. Perdew, K. Burke, and M. Ernzerhof, Phys. Rev. Lett. **77**, 3865 (1996).

[2] S. P. Rudin, M. D. Jones, C. W. Greeff, and R. C. Albers, Phys. Rev. B **65**, 235114 (2002).

[3] S. P. Rudin, M. D. Jones, and R. C. Albers, Phys. Rev. B **69**, 094117 (2004).

[4] I. Schnell and R. C. Albers, J. Phys.: Condens. Matter **18**, 1483 (2006).

[5] H. Xia, S. J. Duclos, A. L. Ruoff, and Y. K. Vohra, Phys. Rev. Lett. **64**, 204 (1990).

[6] E. S. Fisher and C. J. Renken, Phys. Rev. **135**, 482 (1964).

[7] C. Stassis, J. Zarestky, D. Arch, O. D. McMasters, and B. N. Harmon, Phys. Rev. B **18**, 2632 (1978).

[8] B. W. Roberts, J. Phys. Chem. Ref. Data **5**, 730 (1976).

[9] E. W. Collings and J. C. Ho, Phys. Rev. B **4**, 349 (1971).

[10] D. A. Young, *Phase Diagrams of the Elements* (University of California, Berkeley, 1991).

[11] A. Heiming, W. Petry, J. Trampenau, M. Alba, C. Herzig, H. R. Schober, and G. Vogl, Phys. Rev. B **43**, 10948 (1991).

[12] M. J. Mehl and D. A. Papaconstantopoulos, Phys. Rev. B **54**, 4519 (1996).

[13] P. Blaha, K. Schwarz, G. K. H. Madsen, D. Kvasnicka, and J. Luitz, *WIEN2K, An Augmented Plane Wave + Local Orbitals Program for Calculating Crystal Properties* (Karlheinz Schwarz, Techn. Universität Wien, Austria, 2001).

[14] J. E. Dennis, Jr., D. M. Gay, and R. E. Welsch, ACM Trans. Math. Softw. **7**, 348 (1981).

[15] M. D. Jones and R. C. Albers, Phys. Rev. B **66**, 134105 (2002).

[16] N. W. Ashcroft and N. D. Mermin, *Solid State Physics* (Saunders, Philadelphia, 1976).

[17] G. J. Ackland, M. C. Warren, and S. J. Clark, J. Phys.: Condens. Matter **9**, 7861 (1997).

[18] W. Frank, C. Elsässer, and M. Fähnle, Phys. Rev. Lett. **74**, 1791 (1995).

[19] R. E. Cohen, L. Stixrude, and E. Wasserman, Phys. Rev. B **56**, 8575 (1997).

[20] G. Venkataraman, L. A. Feldkamp, and V. C. Sahni, *Dynamics of Perfect Crystals* (MIT Press, Cambridge, MA, and London, England, 1975).

[21] K. Huang, Proc. R. Soc. London, Ser. A **207**, 178 (1950).

[22] J. F. Nye, *Physical Properties of Crystals* (Oxford University Press, New York, 1985).

[23] T. H. K. Barron and M. L. Klein, Proc. Phys. Soc. London **85**, 523 (1965).

[24] L. Fast, J. M. Wills, B. Johansson, and O. Eriksson, Phys. Rev. B **51**, 17431 (1995).

[25] M. Born and K. Huang, *Dynamical Theory of Crystal Lattices* (Clarendon, Oxford, 1954).

[26] S. Wei and M. Y. Chou, Phys. Rev. Lett. **69**, 2799 (1992).

[27] G. Kresse and J. Furthmüller, Comput. Mater. Sci. **6**, 15 (1996); Phys. Rev. B **54**, 11169 (1996).

[28] G. P. Srivastava and K. Kunc, J. Phys. C **21**, 5087 (1988).

[29] F. Reif, *Fundamentals of Statistical and Thermal Physics* (McGraw-Hill, Singapore, 1965).

[30] A. F. Guillermet, High Temp. - High Press. **19**, 119 (1986).

[31] R. R. Hultgren, P. D. Desai, D. T. Hawkins, M. Gleiser, K. K. Kelley, and D. D. Wagman, *Selected Values of the Thermodynamic Properties of Elements* (American Society for Metals, Cleveland, 1973).

[32] Y. Xie and J. A. Blackman, Phys. Rev. B **63**, 125105 (2000); **64**, 195115 (2001).

[33] C. Barreteau, D. Spanjaard, and M. C. Desjonqueres, Phys. Rev. B **58**, 9721 (1997).

[34] S. Baroni, S. de Gironcoli, A. Dal Corso, and P. Giannozzi, Rev. Mod. Phys. **73**, 515 (2001).

[35] J. H. Rose, J. R. Smith, F. Guinea, and J. Ferrante, Phys. Rev. B **29**, 2963 (1984).

[36] *Smithells Metals Reference Book*, 6th ed., edited by E. A. Brandes (Butterworth, London, 1983).

[37] M. J. Mehl, D. A. Papaconstantopoulos, N. Kioussis, and M. Herbranson, Phys. Rev. B **61**, 4894 (2000).